Korean J. Chem. Eng., **31**(2), 240-247 (2014)
DOI: 10.1007/s11814-013-0191-8

pISSN: 0256-1115
eISSN: 1975-7220

Wastewater treatment using photo-impinging streams cyclone reactor: Computational fluid dynamics and kinetics modeling

Sayed Javid Royaee*,†, Morteza Sohrabi, and Amin Shafeghat***

*Refining Technology Development Division, Research Institute of Petroleum Industry, Tehran, Iran
**Chemical Engineering Department, Amirkabir University of Technology, Tehran, Iran
(*Received 20 October 2012 • accepted 30 September 2013*)

Abstract−A photo impinging streams cyclone reactor has been used as a novel apparatus in photocatalytic degradation of organic compounds using titanium dioxide nanoparticles in wastewater. The operating parameters, including catalyst loading, pH, initial phenol concentration and light intensity have been optimized to increase the efficiency of the photocatalytic degradation process within this photoreactor. The results have demonstrated a higher efficiency and an increased performance capability of the present reactor in comparison with the conventional processes. In the next step, residence time distribution (RTD) of the slurry phase within the reactor was measured using the impulse tracer method. A CFD-based model for predicting the RTD was also developed which compared well with the experimental results. The RTD data was finally applied in conjunction with the phenol degradation kinetic model to predict the apparent rate coefficient for such a reaction.

Keywords: Phenol, Photo-impinging Cyclone Reactor, Degradation, TiO_2, RTD, CFD

INTRODUCTION

Effective removal of water pollution is essential in the water treatment process. The pollution removal mechanisms can be classified as chemical oxidation, biochemical treatment, activated carbon adsorption and advanced oxidation processes (AOPs). Photo catalytic technique is classified under AOPs. Such a process has attracted considerable attention within the last few years due to its ability to decompose a wide range of organic and inorganic pollutants at ambient temperature and pressure, without generation of harmful byproducts. [1-4]. In photocatalytic degradation processes, the catalyst suspension method excels over the immobilized or supported catalyst techniques due to the higher efficiency of the former method [5]; however, the requirement of the catalyst separation after the photocatalytic treatment may be regarded as a disadvantage.

In case of heterogeneous photocatalytic processes, the organic compounds present in liquid phase are first degraded to their respective intermediates, and if the irradiation time is further extended are finally mineralized to carbon dioxide and water, (Eq. (1)).

$$\text{Organic Contaminants} \xrightarrow{TiO_2/h\nu} \text{Intermediate} \rightarrow CO_2 + H_2O \quad (1)$$

The overall photocatalytic reaction as described by Eq. (1) can be divided into ve independent steps, [6,7]:

1. Mass transfer of the organic contaminant(s) (e.g., A) in the liquid phase to the TiO_2 surface.

2. Adsorption of the organic contaminant(s) onto the photon activated TiO_2 surface (i.e., surface activation by photon energy occurs simultaneously in this step).

3. Photocatalytic reaction for the adsorbed phase on the TiO_2 surface (e.g., A/B).

4. Desorption of the intermediate(s) (e.g., B) from the TiO_2 surface.

5. Mass transfer of the intermediate(s) (e.g., B) from the interface region to the bulk fluid.

According these steps, there are two essential issues in the case of liquid phase reactions: photon transfer limitations and mass transfer limitations. An ideally intensified reactor, however, should be able to integrate both maximized light efficiency and mass transfer process within a single piece of equipment. On the other hand, only when both mass and photon transfer resistances are overcome can the intrinsic kinetic parameter be studied.

By application of impinging streams cyclone reactors both limitations may be overcome simultaneously for the following reasons [8]:

(a) Increase in relative velocities between the phases.

(b) Increase in the residence time of particles due to oscillatory motion within the impingement zone.

(c) Enhancement of the effective area for mass and heat transfer, which could be nearly identical to the total surface of the particles in the flow.

(d) Potential for excellent mixing within the impingement region, which in turn enhances the overall mass and heat transfer rates.

Residence time distribution (RTD) in a reactor is an important parameter required for design. In an impinging stream reactor, the residence time of particles in the impingement zone is one of the more important issues, as such a zone is the active region in enhancing heat and mass transfer between the phases. The RTD depends on the flow hydrodynamics and the reactor geometry; it has major influence on the reactor chemical performance criteria such as conversion and yield.

The viability of computational fluid dynamics (CFD) for the design and optimization of chemical reactors has been demonstrated extensively for a wide variety of systems [9-13]. An increasing number

†To whom correspondence should be addressed.
E-mail: royaeesj@ripi.ir, sjroyaee@yahoo.com

of studies have reported the use of CFD modeling to estimate values of important properties needed for reactor design, such as the mean residence time of particles, hold-up and residence time distribution in reactors [14-18].

Considering these issues, an impinging streams cyclone reactor has been utilized as a novel apparatus in photocatalytic degradation of phenol as representative organic compound. In the next step, the RTD was simulated using CFD method, and the predicted results compared well with the experimental data.

EXPERIMENTAL

1. Materials

Nanoparticle titanium dioxide (P25) was supplied by Degussa, Germany; nanoparticle zinc oxide was provided by Nano Amor, USA. Phenol with above 99.5% purity, Phenol test kit, Fe^{2+} test kit and COD vials were all obtained from Merck Co. Potassium trioxalatoferrate (III) trihydrate was provided by Alfa Aeser Company.

2. Analytical Procedures

The concentration of phenol was measured by visible spectrophotometer (Dr 2800 Hach Co.) at a wavelength of 495 nm using 4-aminoantipyrine method. Owing to presence of TiO_2 powders in the system, the samples were first filtered using a 0.22 μm syringe filter (Millipore) to remove particles. In addition, the COD of solution was measured at a wavelength of 445 nm using COD vials. The radiation intensity within the photoreactor was determined by ferrioxalate actinometry following the method of Hatchard and Parker [19].

3. Photo-reactor

In the first step, batch circulation photocatalysis experiments were performed to determine the optimum operating conditions. A schematic diagram of the photo-impinging streams reactor used in this step is shown in Fig. 1(a). The apparatus consisted of a cylindrical vessel made of Pyrex and equipped with eight low-pressure mercury vapor lamps, with a dominant emission line at 253.7 nm (TUV 8W from Philips Co.) as irradiation sources at center line of the vessel. The two streams of suspension (TiO_2+Phenol Solution) were fed through symmetrically positioned acceleration pipes. The accelerated suspension feed streams impinged at the annular space and dropped instantly along the inner discharge tube down to the outlet port.

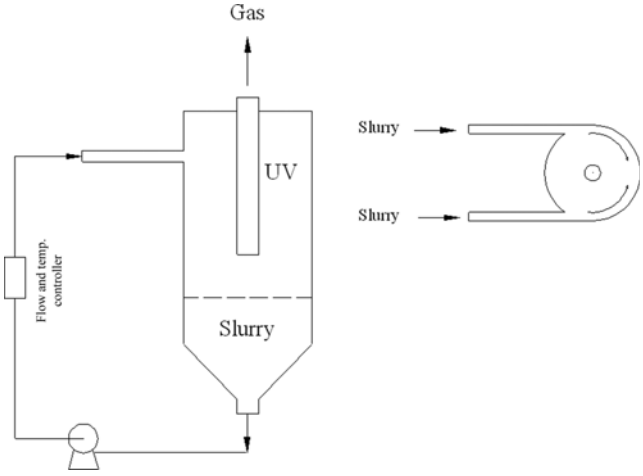

Fig. 1. Schema of photo-impinging streams cyclone reactor.

In a typical experiment, the initial phenol concentration and the amount of suspended TiO_2 were set at 100 mg l^{-1} and 1 g l^{-1}, respectively. A stream of air with a flow rate of 2 L min^{-1} was continuously supplied to the slurry solution. To prevent hole/electron formation, prior to turning on the illumination, the catalyst was placed in the feed reservoir at dark. The phenol solution was then added and the suspension was saturated with air and stirred by pumping the slurry in darkness for 30 min to establish an adsorption-desorption equilibrium. The lamps were then switched on and the suspension, after passing thorough the two nozzles, was irradiated with UV light and collided in the impingement zone. Samples were regularly withdrawn from the reactor and filtered to remove all the suspended solid particles prior to analysis. The pH of the solution was adjusted by adding 0.1 mol l^{-1} NaOH or H_2SO_4 and monitoring with a digital pH meter. The temperature of the photo reactor was maintained at 40±1 °C by a water-cooled jacket around the reactor and feed reservoir.

4. Experimental RTD Determination

The residence time distribution, RTD, one of the major informative characteristics of the flow pattern in a chemical reactor, provides information on the duration of stay of various elements within the reactor and allows for thorough comparison between systems having different configuration of the reactor. For reactor design and scale-up purposes, it is essential to have information on the RTD.

The simplest and most direct way of finding the RTD curve is a physical or nonreactive tracer with pulse injection. In the present study, bulk material was first fed into the reactor until steady state was established. Reactive Black 8 dye as tracer was then injected instantaneously into the inflow stream. Samples were collected at the outlet of the reactor at regular time intervals. The disturbance to the bulk flow caused by the injection of the tracer may be assumed to be negligible. The collected samples were analyzed by uv-visible spectrophotometer to determine the concentration of dye. By measured concentration of tracer at regular time intervals, the residence time distribution curve, the variance (σ^2) and the mean residence time ($\bar{t}_m$) may be determined, using the following relations.

$$E_i = \frac{C_i}{\sum_{i=1}^{27} C_i \Delta t_i} \tag{2}$$

$$\bar{t} = \frac{\sum_{i=1}^{27} t_i C_i \Delta t_i}{\sum_{i=1}^{27} C_i \Delta t_i} \tag{3}$$

$$\sigma^2 = \frac{\sum_{i=1}^{27} (t_i - \bar{t})^2 C_i \Delta t_i}{\sum_{i=1}^{27} C_i \Delta t_i} \tag{4}$$

These parameters may be made dimensionless, applying the following relations:

$$\theta = \frac{t}{\bar{t}},\ E_\theta = \bar{t}E,\ \sigma_\theta^2 = \frac{\sigma^2}{\bar{t}^2} \tag{5}$$

5. RTD Simulating Using CFD

A detailed geometric dimension of photo reactor is shown in Fig. 1. The CFD software package, Fluent of ANSYS Package (V13.0), was used to simulate the photo reactor. Design modeler of Ansys software was used to create the 3D geometry of the photo reactor. In the next step, meshing part of Ansys software was used to mesh the 3D flow domain. To ensure grid independency of the results, four meshes (285324, 349398, 622172 and 863360 elements) were tested for the geometry. The k-ε model was used as turbulent model. The boundary conditions for the CFD model were defined as follows. At the inlet, the mass flow rate of the fluid was specified. The direction of the flow was defined normal to the boundary. The hydraulic diameter was fixed at 20 mm and the turbulence intensity (TI) was set with values close to 5%. The TI was estimated based on the formula $TI=0.16\ Re^{-1/8}$ [20]. At the outlet, a fully developed flow (outflow) condition was applied. The standard wall function was employed for the turbulent boundary layer in the wall region.

The solver was set up for unsteady state, coupled and implicit model with considering gravity force to solve the governing equations, starting with second-order upwind formulation for the converged solution. The SIMPLE method was chosen for the pressure-velocity coupling. The convergence of the numerical solution was ensured by monitoring the scaled residuals of continuity, x, y and z velocities components, and the turbulence parameters to a value of less than 10^{-6}. A UDF was also written for injecting the impulse tracer.

RESULTS AND DISCUSSION

Certain pertinent operating parameters in heterogeneous photocatalytic reactions are the type of catalyst, catalyst loading, substrate concentration, pH and light intensity [21,22]. Stream flow rates are a crucial parameter in the design of impinging stream reactors. Investigation of the continuous treatment is essential for evaluation of the performance capability of the wastewater treatment system.

1. Effect of Flow Rate

To study the effect of flow rate on the efficiency of the impinging streams cyclone reactor, a range of flow rates (20, 30, 40, 50, 55 l min^{-1}) were applied. Results presented in Fig. 2 may indicate that at low flow rates, the degradation of phenol did not exceed 20% after 4 hours. This may be explained by noting that at low flow rates, the intensity of collisions is reduced and as such, the irradiation absorbed by the solution is decreased. Consequently, conversion is low. While at higher flow rates the collision rate, turbulence of flow and renewal of catalyst surface are all enhanced, and thus, the irradiation absorbed by the slurry within a fixed period of time is promoted. These phenomena lead to a higher degradation rate. Regarding the results obtained, the optimum flow rate of phenol solution was selected as 50 l min^{-1}.

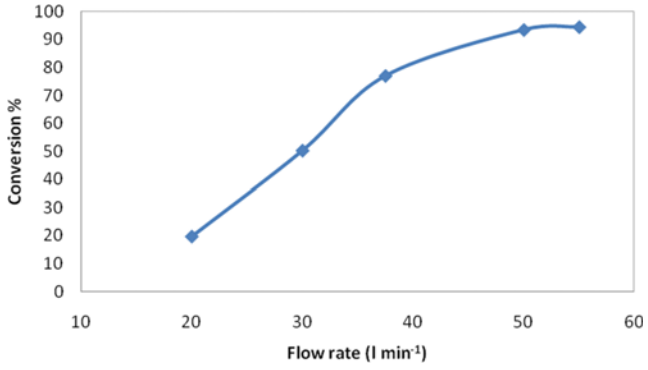

Fig. 2. Effect of flow rate on photo catalytic degradation of phenol (reaction time: 240 min). [PhOH].=100 mg l^{-1}, Catalyst loading=1 g l^{-1}, Temperature=40 °C, pH=Natural value.

2. Type of Catalyst

A number of semiconductors have been were examined and applied as photocatalysts for the degradation of organic contaminants [21,23,24]. Among the semiconductors employed, both TiO_2 and ZnO demonstrated a number of advantages as photocatalysts. These compounds are inexpensive, non-toxic and highly effective [25]. Preliminary experiments were thus carried out to examine the activity of the selected catalysts for degradation of phenol. The results indicated a higher photocatalytic activity of TiO_2 compared with ZnO (Fig. 3). Hence, TiO_2 was selected as a suitable catalyst and applied in the process. Optimization of certain key parameters of the photodegradation of phenol was carried out using such a catalyst.

3. Effect of Catalyst Loading

To avoid an ineffective excess of catalyst within the system and to ensure total absorption of efficient photons, the optimum mass of catalyst has to be found [21,26,27]. To determine the optimal loading of photocatalyst, various amounts of P25 TiO_2 (0.5-2.0 g l^{-1}) were mixed with 100 mg l^{-1} of phenol solutions. Fig. 3(a) shows the results at natural pH value. In Fig. 3(a) UV irradiation in the absence of TiO_2 catalyst (i.e., direct photolysis) results in a low re-

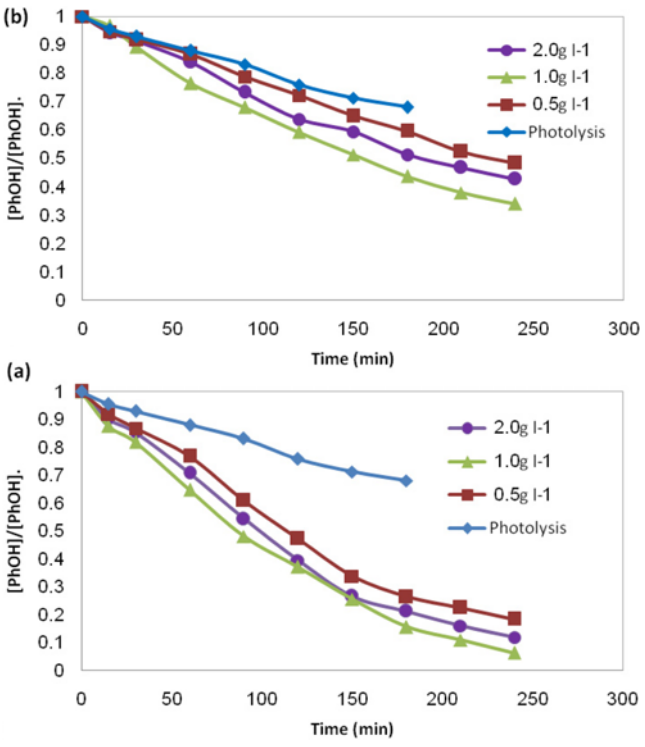

Fig. 3. Effect of catalyst loading on the photo catalytic degradation of phenol, (a) TiO_2, (b) ZnO. [PhOH].=100 mg l^{-1}, Temperature=40 °C, pH=Natural value.

moval of phenol. However, when TiO_2 loading was increased from 0.5 to 1 g l^{-1}, the photodegradation was enhanced from 81 to 94% after 4 h. However, further increase in TiO_2 loading led to a slight decrease in phenol removal.

Results from extensive studies have demonstrated that the rates of photodegradation for organic pollutants are strongly affected by the number of active sites and the photo-absorption ability of the catalyst used [27,28]. Increased loading of the catalyst increases the generation rate of electron/hole pairs and, thus, formation of $^{\bullet}OH$ radicals leading to the enhancement of photodegradation. On the other hand, an excess of catalyst decreases the light penetration due to shielding by the suspended particles [26,29], causing reduction of the rate of photodegradation. Such a rate reduction may be also attributed to the screening effect of the redundant dispersion of UV radiation as the result of substantial amount of suspended photocatalyst. Furthermore, under these conditions particles tend to agglomerate, making a significant fraction of the catalyst inaccessible to either adsorbing the molecules or absorbing the radiation, with consequent decrease in the active sites available to the catalytic reaction. Thus, a balance exists between these two opposing effects that result in an optimum catalyst loading of 1.0 g l^{-1} ZnO providing the maximum efficiency.

Owing to the highly turbulent condition of slurry in this reactor, increased loading of TiO_2 leads to formation of foam within the reactor creating a pumping problem and reduces the photodegradation rate.

4. Effect of pH

As expected, TiO_2 exhibits amphoteric behavior in aqueous media. The point of zero charge (pzc) of TiO_2 P25, i.e., the point when the surface charge density is zero, is reported to be between 6.2 and 6.8 [26,30,31]. This means that the surface of the catalyst is positively charged at $pH<pH_{pzc}$ (Eq. (6)), negatively charged at $pH>pH_{pzc}$ (Eq. (7)), and remains neutral at $pH=pH_{pzc}$:

$$TiOH+H^{+} \rightarrow TiOH_2^{+} \quad (6)$$

$$TIOH+OH^{-} \rightarrow TiO^{-}+H_2O \quad (7)$$

where, $TiOH_2^{+}$, TiOH, and TiO^{-} are the positive, neutral, and negative surface hydroxyl groups, respectively. Such a behavior significantly affects not only the adsorption-desorption properties of TiO_2 surface, but also the changes of the pollutant structure at various pH values. In aqueous media, phenol has a pK_a of 9.9 (at 25 °C), indicating that in solutions with $pH<P_{Ka}$, phenol is in the molecular form (C_6H_5OH). Whereas, at $pH>P_{Ka}$ the phenol molecule undergoes deprotonation, becoming negatively charged (C_6H_5O) [26,27,29]. Thus, electric charge properties of both catalyst and substrate play an important role in the adsorption process, i.e., the interaction and affinity between both TiO_2 and phenol will vary with the solution pH.

The pH of the suspensions was varied to study the effect of this parameter on the photocatalytic degradation of phenol. As it may be observed from Fig. 4, decrease in pH from natural pH value (about 5.8) to 3.5 has no appreciable effect on the process. However, at pH 11.5, the photoefficiency of the process decreases drastically, and phenol removal becomes extremely slow. Under such conditions, both catalyst and substrate are negatively charged and thus, repulsive forces are generated between the two, leading to the reduction of substrate adsorption. With either acidic or basic conditions of the starting solutions, it was observed that with continuation of the reaction, the solution pH tended to neutral value. In addition, with both acidic and neutral initial solutions the rate of degradation was almost identical. However, when the initial solution was basic, the rate of phenol removal was usually retarded. Such an observation may indicate an initial low acidic condition for effective phenol degradation.

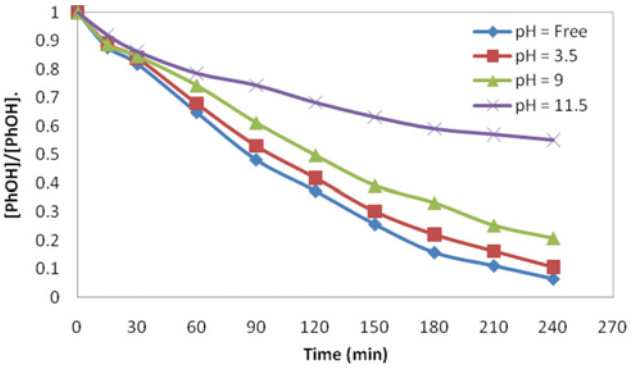

Fig. 4. Effect of pH on the photo catalytic degradation of phenol. [PhOH].=100 mg l^{-1}, Catalyst loading=1 g l^{-1}, Temperature= 40 °C.

5. Effect of the Initial Phenol Concentration

It is important both from a mechanistic and an application point of view to study the dependency of the photocatalytic reaction rate on the substrate concentration. Thus, the initial phenol concentration (prior to the adsorption in dark) was varied from 20 to 100 mg l^{-1}. Results showed that beyond this range of concentrations, any increase in phenol quantity, may lead to the decrease in degradation rate (Fig. 5). By increasing the phenol concentration, higher amounts of reactant and reaction intermediates are adsorbed at the surface of the photocatalyst, and thus the generation of hydroxyl radicals declines due to the reduction in the number of active sites available for adsorption of hydroxyl anions. On the other hand, when the phenol concentration is low, while the catalyst loading and light intensity are kept unchanged, larger numbers of active sites and hydroxyl radicals are available to intermediates. As a consequence, the total COD of solution decreases sharply (Fig. 6). In addition, during photocatalytic oxidation, the decomposition of the organic substrate is

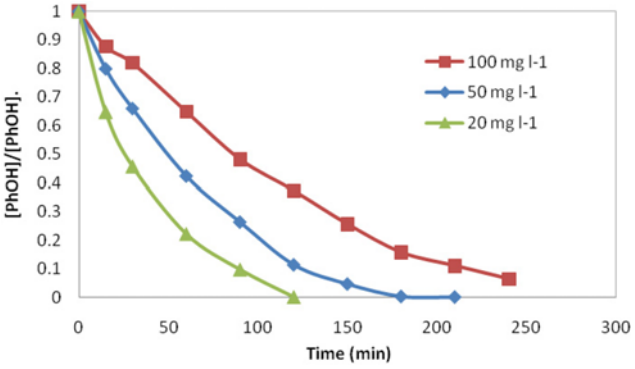

Fig. 5. Effect of the initial concentration of phenol on the reaction time. Catalyst loading=1 g l^{-1}, Temperature=40 °C, pH= Natural value.

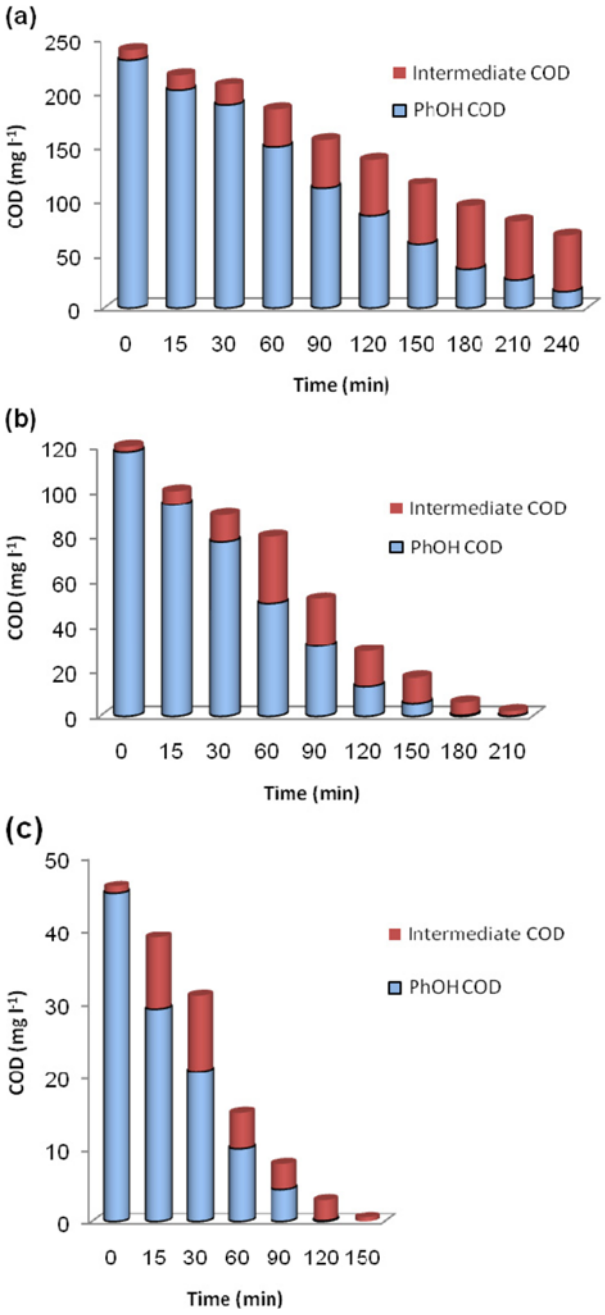

Fig. 6. Effect of the initial concentration of phenol on COD removal. Catalyst loading=1 g l^{-1}, Temperature=40 °C, pH=Free, (a) [PhOH].=100 mg l^{-1}, (b) [PhOH].=50 mg l^{-1}, (c) [PhOH].=20 mg l^{-1}.

dependent upon photonic efficiency. At high-substrate concentrations, however, the photonic efficiency diminishes and the titanium dioxide surface becomes saturated with the substrate and intermediates, leading to catalyst deactivation [32].

6. Effect of Light Intensity

The rate of photocatalytic reactions depends largely on the radiation absorption of the photocatalyst. A review by Ollis et al. [33] on the effect of light intensity upon the kinetics of the photocatalytic process demonstrated that (i) at low light intensities (0-20 mW cm^{-2}), the rate would increase linearly with increasing light intensity (first order); (ii) at intermediate light intensities, beyond a certain value (approximately 25 mW cm^{-2}), the rate would depend on the square root of the light intensity (half order), and (iii) at high light intensities the rate would level off to become independent from the light intensity. Such an observation may be interpreted as follows: at low light intensity, reactions involving electron-hole formation predominate while the electron-hole recombination is negligible. However, as the light intensity is increased, electron-hole pair separation competes with electron-hole recombination, retarding the reaction rate.

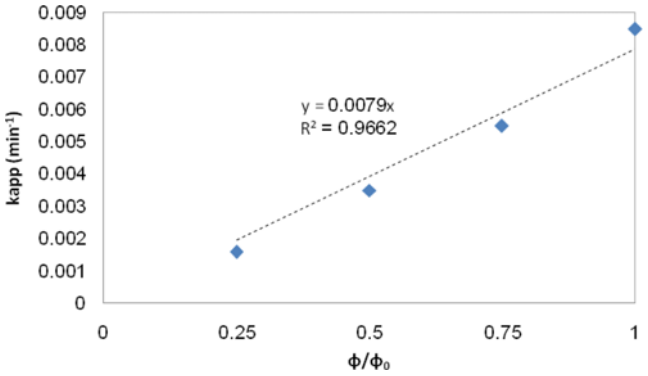

Fig. 7. Initial reaction rates as a function of light intensity. [PhOH]. =100 mg l^{-1}, Catalyst loading=1 g l^{-1}, Temperature=40 °C, pH=Natural value.

To study the influence of different light intensity on the photocatalytic degradation of phenol, the photoreactor was equipped with eight low-pressure mercury vapor lamps. A number of experiments were carried out, applying various light intensities generated from 2, 4, 6 and 8 lamps. Radiation intensities were determined by ferrioxalate actinometry and are here presented as fractions of the initial photonic flow. Within the range of intensities studied, the initial rates were observed to change linearly with the photonic flow (Fig. 7). The slope of the line shows reaction rate increasing versus increasing of light intensity.

7. Experimental RTD

To perform RTD experiments, a circular plate divided into 80 equal cells was constructed. The plate was placed under the discharge port of the reactor and was being driven at the selected speed by means of an electric motor. Since UV light has no effect on the hydrodynamics of the reactor, RTD studies were performed in the absence of UV light in order to hinder any interaction between UV light and the tracer. By measuring the concentration of tracer in each cell, the age distribution [E(t)], the variance (σ^2) and the mean residence time ($\bar{t}_m$) can be calculated. Plots of E(t) versus nΔt as the experimental RTD curve are presented in Fig. 8.

8. CFD Simulation for RTD Determination

In Fig. 8, a comparison has been made between the results obtained from simulated RTDs using different mesh type and the experimental RTD. As it may be observed from this figure, 4th mesh type is independent from the number of cells of the grid and there is a good correlation between the predicted data and those determined by the experimental study for it. So, this CFD setup may be used for case study of design parameter such as inlet velocity or nuzzle diameter.

Fig. 9 shows the stream line patterns within the reactor. After the

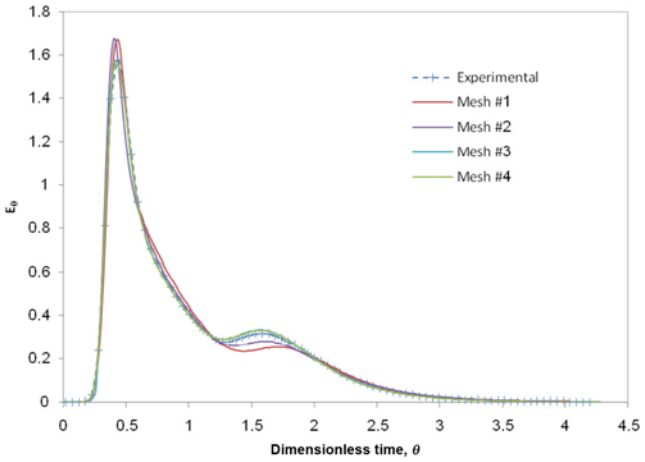

Fig. 8. Dimensionless RTD curves, experimental and simulated.

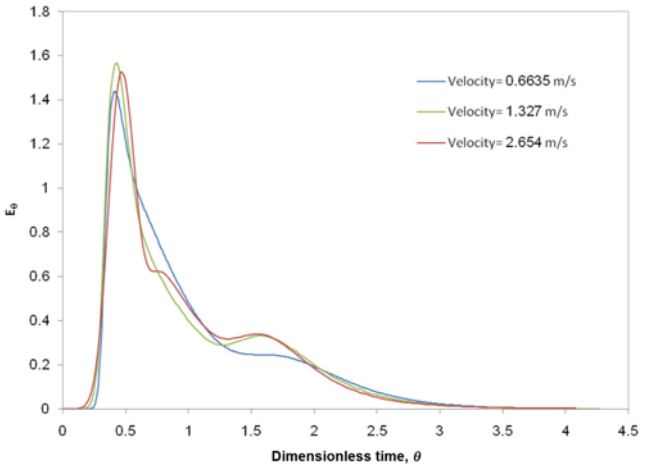

Fig. 10. Effect of inlet velocity on RTD.

collision, a part of the flow rises and then breaks down from the front of the reactor after twisting on the walls. It causes a second peak to be created in the RTD curve.

9. Effect of Inlet Velocity

To investigate the effect of changes in inlet velocity on RTD and mean residence time, three velocities, 0.6635, 1.327 and 2.654 m s^{-1}, were chosen. As can been seen in Fig. 10, with increasing inlet velocity the tracer lead to outlet earlier and due to further twisting of the fluid on the walls, the number of peaks in RTD becomes more. Fig. 11 shows the changes of mean residence time due to inlet velocity. Increasing inlet velocity decreases mean residence time nonlinearly.

10. Kinetic Study

The pseudo-first-order kinetics with an apparent first-order rate constant is usually applied to describe the kinetics of photocatalytic reactions of aquatic organics [1,4,26,27,34].

$$C_p = C_{p0} e^{-k_r K_{ad} t} = C_{p0} e^{-k_{app} t} \tag{8}$$

where, C_{P0} is the initial concentration at t=0.

Concentration of phenol after the first pass of reactants through the reactor may be calculated as follows [35],

$$C_{P_{r,out}} = \int_0^\infty (C_p)_b E dt = \sum_i (C_p)_b E_i \Delta t_i \tag{9}$$

A balance around the feed reservoir in Fig. 1 may be set up as follows:

$$Q_r C_{P_{r,out}} - Q_r C_{P_{r,in}} = \frac{d(V_F C_{P_r})}{dt} \tag{10}$$

where V_F, is the volume of phenol solution in feed reservoir and Q_r, is the volume flow rate of feed to the reactor.

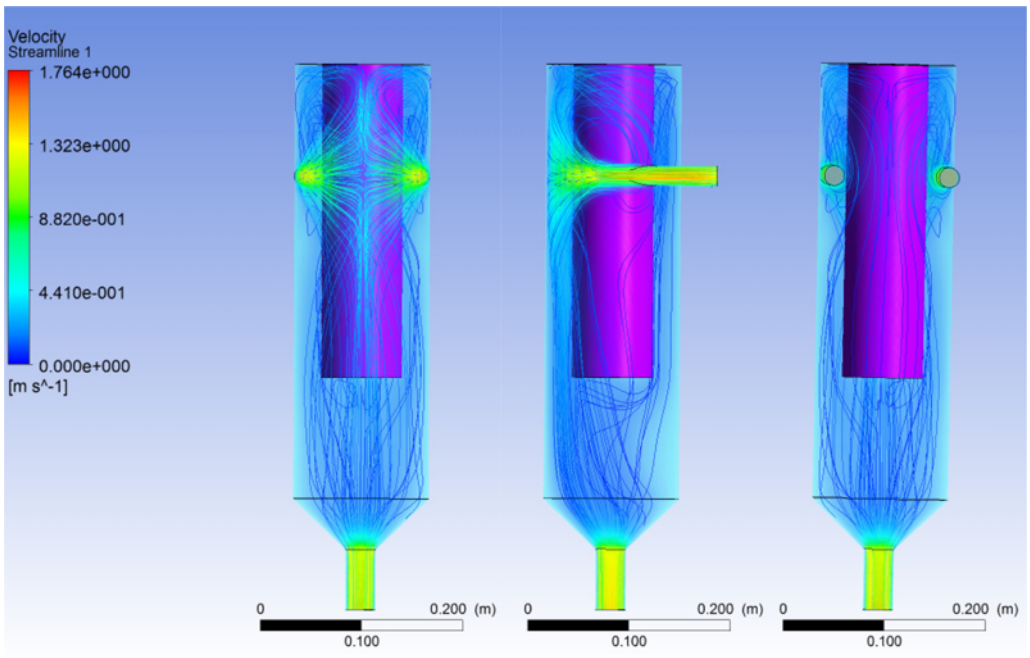

Fig. 9. Stream line patterns within the reactor.

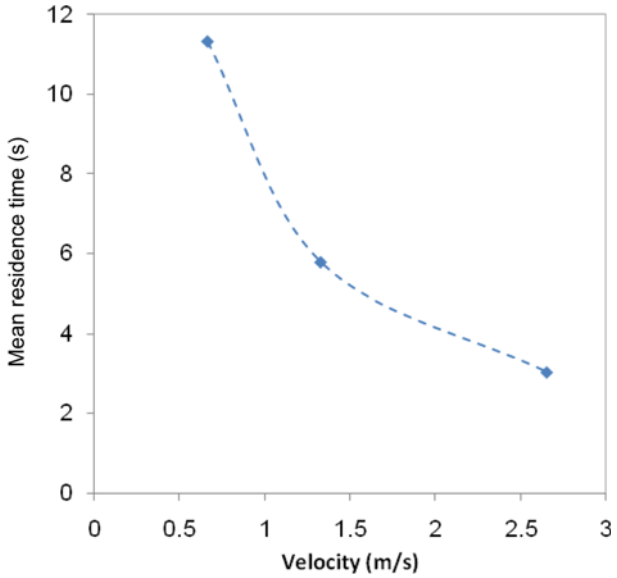

Fig. 11. Effect of inlet velocity on mean residence time.

The above relation may be replaced by the finite difference form.

$$Q_r(C_{P_{r,out}} - C_{P_{r,in}}) = V_F \frac{C_{P_t}^{n+1} - C_{P_t}^{n}}{\bar{t}} \quad (11)$$

where, $\bar{t}$, is the mean residence time and n=t/$\bar{t}$.

Combining Eq. (9) and (11) and assuming a pseudo-first-order kinetics,

$$\frac{C_{P_c}^{n+1}}{C_{P_c}^{n}} = \frac{Q_r}{V_F}\bar{t}\sum_i e^{-k_{app}\Delta t_i} E_i \Delta t_i + \left(1 - \frac{Q_r}{V_F}\bar{t}\right) \quad (12)$$

Therefore,

$$\frac{C_{P_c}^{n+1}}{C_{P_t}^{0}} = \prod_n \frac{Q_r}{V_F}\bar{t}\sum_i e^{-k_{app}\Delta t_i} E_i \Delta t + \left(1 - \frac{Q_r}{V_f}\bar{t}\right) \quad (13)$$

or

$$1 - X_{n+1} = \frac{C_{P_c}^{n+1}}{C_{P_r}^{0}} = \left(\frac{Q_r}{V_F}\bar{t}\sum_i e^{-k_{app}\Delta t_i} E_i \Delta t + \left(1 - \frac{Q_r}{V_f}\bar{t}\right)\right)^n, \ \Delta t = \text{constant} \quad (14)$$

Table 1. Apparent rate coefficients and SEEs

Phenol concentration (mg l^{-1})	100	50	20
k (min^{-1})	0.0442	0.0815	0.1444
SEE	0.0122	0.0087	0.0060

Now, the apparent first-order rate coefficient may be determined from the above relation for the reactions carried out in a PISCR. In case of phenol degradation, certain experimental runs were carried out with different initial concentrations of phenol.

To determine the apparent rate coefficient, the data predicted from the proposed model were compared with those obtained experimentally under identical operating conditions applying the Levenberg-Marquardt non-linear regression method. The parameters were optimized according to the following objective function:

$$SSE = \sum_i Err_i^2 = \sum_i (X_i - \hat{X}_i)^2 \quad (15)$$

where, SSE is the sum of the square errors for each component, $\hat{X}_i$ is the experimental conversions and X_i is the conversion values calculated from Eq. (14). In Table 1 the apparent rate coefficients and sum of the square errors are presented for optimum condition. The estimated values are much higher than those available in the literature [1,4,26,27,34,36]. The results of the present study and reported data are compared in Table 2. This may be explained by the severe mass transfer limitations affecting the performance of conventional reactors.

CONCLUSION

Regarding the present observations, it seems that by application of a photo-impinging streams cyclone reactor (PISCR) the photon and mass transfer limitation are both eliminated, leading to a higher efficiency for phenol degradation. Results showed that during 4 h reaction time in presence of TiO_2, phenol was completely decomposed. With regard to the higher concentration of phenol (3 L solution containing 100 mg L^{-1} phenol) and the lower degradation time observed in the present study in comparison with reported data [1, 24,26,27,36] the higher performance capability of the PISCR may

Table 2. Comparison of present study with the reported data

Light source	Solution volume ml	Phenol concentration mg l^{-1}	Catalyst loading g l^{-1}	Time of degradation	Conversion %	K_{app} (min^{-1})	References
Eight low-pressure mercury vapor lamps (8 W, 253.7 nm)	3000	100	1 / Tio2	4 h	96.4	0.0442	This work
A high-pressure mercury lamp (400 W, 365 nm)	800	48	1 / Tio2	3 h	50	0.0049	26
A Heraeus TNN 15/32 low-pressure mercury vapor lamp (253.7 nm)	800	50	1 / Tio2	4 h	100	0.0204	27
Sixteen phosphor-coated low-pressure mercury lamps (300 nm)	360 (3*120)	100	1 / Tio2	3.5 h	100	0.02	1
A medium-pressure mercury lamp (125 W, 254 nm)	200	94	1 / Tio2	4 h	98.4	0.0151	34
A high-pressure mercury lamp (400 W, 365 nm)	800	67	1 / Tio2	3 h	35	0.0027	36

be established.

The photocatalytic process is influenced by several design and operating parameters, including feed flow rate, catalyst loading, initial phenol concentration, pH of the medium and irradiation intensity. The maximum degradation rate of phenol was observed in case of approximately neutral solutions.

RTD of the photo-impinging streams cyclone reactor has been determined experimentally by impulse tracer analysis. The CFD method can be used as a proper tool for simulation and optimization of the processes carried out in PISCR. A good correlation was observed between the predicted and experimental RTD.

The RTD data was used in conjunction with phenol photo degradation rate equation to predict the rate coefficient of this reaction conducted in a photo-impinging system as the chemical reactor. The estimated values were much higher than those available in the literature. The lower values for the apparent rate coefficients determined under conventional conditions, may be related to the limitations imposed by the external and internal diffusion resistances on the overall rate of reaction and, hence, on the apparent rate coefficients. Whereas, in impinging streams systems, mass transfer resistances are expected to be substantially lower than those present in conventional apparatus.

REFERENCES

1. S. Ray, J. A. Lalman and N. Biswas, *Chem. Eng. J*., **150**, 15 (2009).
2. M. B. Ray, J. P. Chen, L. K. Wang and S. O. Pehkonen, Handbook of Environmental Engineering, Volume 4, *Advanced physicochemical treatment processes*, Chapter 14, Advanced Oxidation Processes, Springer (2007).
3. F. Shahrezaei, Y. Mansouri, A. A. L. Zinatizadeh and A. Akhbari, *Powder Technol.*, **221**, 203 (2012).
4. K. Elghniji, O. Hentati, N. Mlaik, A. Mahfoudh and M. Ksibi, *J. Environ. Sci*., **24**, 479 (2012).
5. D. Gumy, A. G. Rincon, R. Hajdu and C. Pulgarin, *Sol. Energy*, **80**, 1376 (2006).
6. J. M. Herrmann, *Catal*. *Today*, **53**, 115 (1999).
7. H. S. Fogler, Elements of Chemical Reaction Engineering, Prentice-Hall PTR Inc., 581 (1999).
8. S. J Royaee and M. Sohrabi, *Desalination*, **253**, 57 (2010).
9. L. Hjertager, B. H. Hjertager and T. Solberg, *Comput*. *Chem*. *Eng*., **26**, 507 (2002).
10. D. L. Marchisio and A. A. Barresi, *Chem*. *Eng*. *Sci*., **58**, 3579 (2003).
11. D. A. Sozzi and F. *Int. J. Heat Fluid Flow*, **27**, 1043 (2006).
12. V. V. Ranade, *Computational flow modeling for chemical reactor engineering*, Academic Press, New York (2002).
13. S. J. Wang, S. Devahastin and A. S. Mujumdar, *Appl*. *Therm*. *Eng*., **26**, 519 (2006).
14. F. Ghirelli, S. Hermansson, H. Thunman and B. Leckner, *Prog*. *Comput*. *Fluid Dyn*., **6**, 241 (2006).
15. S. Vedantam, J. B. Joshi, S. B. Koganti, *Ind. Eng. Chem. Res*., **45**, 6360 (2006).
16. V. A. Atiemo Obeng, E. L. Paul and S. M. Kresta, *Handbook of industrial mixing: Science and practice*, Wiley-IEEE (2004).
17. B. S. Choi, B. Wan, S. Philyaw, K. Dhanasekharan and T. A. Ring, *Ind. Eng. Chem. Res*., **43**, 6548 (2004).
18. B. S. Choi, B. Wan, S. Philyaw, K. Dhanasekharan and T. A. Ring, *Residence time distributions in a stirred tank-comparison of CFD predictions with experiment*, in: Proceedings of the AIChE Annual Meeting (2007).
19. C. G. Hatchard and C. A. Parker, *Proc. R. Soc., London, Ser. A*, **235**, 518 (1956).
20. J. Esteban Duran, *Chem. Eng. Sci.*, **65**, 1201 (2010).
21. T. V. Gerven, G. Mulc, J. Moulijn and A. Stankiewicz, *Chem. Eng. Process*, **46**, 781 (2007).
22. J. M. Herrmann, *Top. Catal.*, **34**, 49 (2005).
23. I. K. Konstantinou, V. A. Sakkas and T. A. Albanis, *Water Res.*, **36**, 2733 (2002).
24. S. K. Pardeshi and A. B. Patil, *Sol. Energy*, **82**, 700 (2008).
25. S. Li, Z. Ma, J. Zhang, Y. Wu and Y. Gong, *Catal. Today*, **139**, 109 (2008).
26. C. H. Chiou, C. Y. Wu and R. S. Juang, *Chem. Eng. J.*, **139**, 322 (2008).
27. C. G. Silva and J. L. Faria, *J. Mol. Catal. A: Chem.*, **305**, 147 (2009).
28. S. Lathasree, A. N. Rao, B. SivaSankar, V. Sadasivam and K. Rengaraj, *J. Mol. Catal. A: Chem.*, **223**, 101 (2004).
29. A. Sobczynski, L. Duczmal and W. Zmudzinski, *J. Mol. Catal. A: Chem.*, **213**, 225 (2004).
30. K. Pujara, S. P. Kamble and V. G. Pangarkar, *Ind. Eng. Chem. Res.*, **46**, 4257 (2007).
31. S. Sakthivel, B. Neppolian, M. V. Shankar, B. Arabindoo, M. Palanichamy, V. Murugesan, *Sol. Energy Mater. Sol. C.*, **77**, 65 (2003).
32. J. Aran, J. L. M. Nieto, J. A. H. Melian, J. M. D. Rodriguez, O. G. Diaz, J. P. Perna, C. A. Bergasa and J. Mendez, *Chemosphere*, **55**, 893 (2004).
33. D. F. Ollis, E. Pelizzetti and N. Serpone, *Environ. Sci. Technol.*, **25**, 1523 (1991).
34. S. N. Hosseini, S. M. Borghei, M. Vossoughi and N. Taghavinia, *Appl. Catal. B: Environ.*, **74**, 53 (2007).
35. M. Sohrabi and M. Ahmadi Marvast, *Ind. Eng. Chem. Res*., **39**, 1903 (2000).
36. C. H. Chiou, C. Y. Wu and R. S. Juang, *Sep. Purif. Technol.*, **62**, 559 (2008).